

Efficient realization of daytime radiative cooling with hollow zigzag SiO_2 metamaterials

Huawei Yao(姚华伟), Xiaoxia Wang(王晓霞), Huaiyuan Yin(殷怀远), Yuanlin Jia(贾渊琳), Yong Gao(高勇), Junqiao Wang(王俊俏), and Chunzhen Fan(范春珍)

Citation: Chin. Phys. B, 2021, 30 (**6**): 064214. DOI: 10.1088/1674-1056/abd697
Journal homepage: http://cpb.iphy.ac.cn; http://iopscience.iop.org/cpb

What follows is a list of articles you may be interested in

Active metasurfaces for manipulatable terahertz technology

Jing-Yuan Wu(吴静远), Xiao-Feng Xu(徐晓峰), Lian-Fu Wei(韦联福)
Chin. Phys. B, 2020, 29 (**9**): 094202. DOI: 10.1088/1674-1056/aba613

Low-power electro-optic phase modulator based on multilayer graphene/silicon nitride waveguide

Lanting Ji(姬兰婷), Wei Chen(陈威), Yang Gao(高阳), Yan Xu(许言), Chi Wu(吴锜), Xibin Wang(王希斌), Yunji Yi(衣云骥), Baohua Li(李宝华), Xiaoqiang Sun(孙小强), Daming Zhang(张大明)
Chin. Phys. B, 2020, 29 (**8**): 084207. DOI: 10.1088/1674-1056/ab943b

A compact electro-absorption modulator based on graphene photonic crystal fiber

Guangwei Fu(付广伟), Ying Wang(王颖), Bilin Wang(王碧霖), Kaili Yang(杨凯丽), Xiaoyu Wang(王晓愚), Xinghu Fu(付兴虎), Wa Jin(金娃), Weihong Bi(毕卫红)
Chin. Phys. B, 2020, 29 (**3**): 034209. DOI: 10.1088/1674-1056/ab6838

Diurnal cooling for continuous thermal sources under direct subtropical sunlight produced by quasi-Cantor structure

Jia-Ye Wu(吴嘉野), Yuan-Zhi Gong(龚远志), Pei-Ran Huang(黄培然), Gen-Jun Ma(马根骏), Qiao-Feng Dai(戴峭峰)
Chin. Phys. B, 2017, 26 (**10**): 104201. DOI: 10.1088/1674-1056/26/10/104201

Infrared emissivities of Mn, Co co-doped ZnO powders

Yao Yin-Hua, Cao Quan-Xi
Chin. Phys. B, 2012, 21 (**12**): 124205. DOI: 10.1088/1674-1056/21/12/124205

Efficient realization of daytime radiative cooling with hollow zigzag SiO_2 metamaterials*

Huawei Yao(姚华伟)[1], Xiaoxia Wang(王晓霞)[1], Huaiyuan Yin(殷怀远)[1], Yuanlin Jia(贾渊琳)[1], Yong Gao(高勇)[2], Junqiao Wang(王俊俏)[1], and Chunzhen Fan(范春珍)[1,†]

[1] *School of Physics and Microelectronics, Zhengzhou University, Zhengzhou* 450001, *China*
[2] *Department of Physics, Shanghai Polytechnic University, Shanghai* 201209, *China*

(Received 20 November 2020; revised manuscript received 11 December 2020; accepted manuscript online 24 December 2020)

A tunable selective emitter with hollow zigzag SiO_2 metamaterials, which are deposited on Si_3N_4 and Ag film, is proposed and numerically investigated for achieving excellent radiative cooling effects. The average emissivity reaches a high value of 98.7% in the atmospheric window and possesses a high reflectivity of 92.0% in the solar spectrum. To reveal the enhanced absorptivity, the confined electric field distribution is investigated, and it can be well explained by moth eye effects. Moreover, tunable emissivity can also be initiated with different incident angles and it stays above 83% when the incident angle is less than 80°, embodying the excellent cooling performance in the atmospheric transparency window. Its net cooling power achieves 100.6 $W{\cdot}m^{-2}$, with a temperature drop of 13°, and the cooling behavior can persist in the presence of non-radiative heat exchange conditions. Therefore, high and tunable selective emitters based on our designed structure could provide a new route to realizing high-performance radiative cooling. This work is also of great significance for saving energy and environmental protection.

Keywords: daytime radiative cooling, hollow zigzag metamaterials, net cooling power, emissivity

PACS: 42.79.Hp, 78.67.Pt, 44.40.+a **DOI:** 10.1088/1674-1056/abd697

1. Introduction

With the increasing demands of modern refrigeration, the corresponding emission of greenhouse gases poses a threat to people's lives, especially from traditional refrigeration methods such as air conditioners which consume a lot of electric energy and generate net heat, which further aggravates CO_2 emission and increases temperatures. It is becoming extremely urgent to find an effective method to reduce temperatures and energy consumption. Recently, the passive cooling technique has aroused widespread interest, which can reduce the target object temperature below the ambient one without any energy consumption. It is regarded as an alternative way to achieve effective cooling, in which refers to reflecting the sunlight in the solar spectrum and pumping heat from objects to cold outer space via the atmospheric window.[1–3] Catalanotti *et al.* realized a selective surface at the atmospheric window and demonstrated practical cooling during nighttime operation in 1975.[4] Since then, nighttime coolers have been extensively studied and improved cooling performances were reported.[5–10] However, to achieve selective radiation in daytime, the radiative cooler needs to have approximately unit reflection at the solar spectrum and high emission at the atmospheric window while considering the non-radiative condition.[11,12]

In order to meet the necessary requirements, a multilayer structure,[13] a photonic metamaterials structure[14–18] and a random particle structure[19,20] were proposed to achieve daytime cooling. Rephaeli *et al.* achieved a metal–dielectric photonic structure to get high-performance daytime radiative cooling.[21] Raman *et al.* proposed a seven alternating layers of SiO_2 and HfO_2 on the top of Ag layer which had a reflectivity of 97%. They experimentally verified 4.9 °C of cooling temperature under direct sunlight in 2014.[22] Chen *et al.* proposed a three-layer radiator with silicon nitride, amorphous silicon and aluminum, which achieved an average temperature reduction of 37 °C by eliminating parasitic thermal load.[23] Kecebas *et al.* investigated a similar periodic radiator with a seven-layer structure and replaced the top layer with Al_2O_3 to improve the net cooling power.[24] Jeong *et al.* put forward a structure with eight alternating layers of SiO_2 and TiO_2, and the average emissivity was 84% in the atmospheric window.[25] The combination of polymer layers such as PDMS,[26] PMMA[27] and PTFE[28] has also been tested for daytime radiative cooling. Photonic metamaterials could prevent high solar absorption in the solar spectrum with a large emissivity in the atmospheric window. Wu *et al.* designed a two-dimensional antenna composed of a low loss alternating Al_2O_3 and SiO_2 multi-layer structure, which possessed both selective MIR emissivity and low solar absorption.[29] Zhu *et al.* proposed a micro photonic design consisting of a two-dimensional silica pyramid array and a 100 μm-thick uniform silica layer atop the bare solar cell.[30] Jeong *et al.* presented a periodic multilayer structure based on PDMS, which verified that patterned metamaterials could obtain high emission.[31] Gentle *et al.* reported that embedded microparticles into polymer could also achieve a radiative cooling effect in 2010.[32] In

*Project supported by the Natural Science Foundation of Henan Educational Committee (Grant No. 21A140026).
†Corresponding author. E-mail: chunzhen@zzu.edu.cn
© 2021 Chinese Physical Society and IOP Publishing Ltd

the subsequent research, random SiO_2 or TiO_2 microparticles in a polymer layer exhibited superior performance for daytime radiative cooling with high emissivity in the atmospheric window and low absorptivity in the solar spectrum region.[33–35] Although much progress had been achieved in the previous works, it is still difficult to realize ideal broadband selective absorption in the atmospheric window with a simple inorganic radiative cooler. Thus, it is necessary to design photonic metamaterials to improve their emissivity and maintain high reflectivity.

In this study, we have proposed a novel metamaterial to achieve a broadband absorption spectrum, which incorporates a patterned SiO_2 layer and Si_3N_4 and Ag layers. The radiative cooler exhibits an average reflection of 92.0% in the solar spectral region and an average emissivity of 98.7% in the atmospheric window simultaneously. The electric field distributions at the resonant peak positions are carefully examined to figure out the origin of the high emissivity. Tunable average emissivity of our proposed structure is explored in detail with different geometric parameters and incident angles. Finally, cooling performance in the steady and transient state is examined respectively and its cooling ability persists when considering non-radiative heat exchange.

2. Model and method

2.1. Model design

Figure 1(a) depicts the three-dimensional configuration of our designed radiative cooler, which consists of hollow zigzag SiO_2 metamaterials deposited on Si_3N_4 and silver substrate. The Si_3N_4 and SiO_2 has extremely low loss in the solar spectrum and a strong absorption peak in the atmospheric window,[36] serving as the absorptive segments. The hollow zigzag structure with a gradual refractive index is designed to improve the anti-reflection performance of the proposed model. Figure 1(b) is the cross-section view of the metamaterials and the geometric parameters are clearly indicated. The periodicity is taken as 7 μm along the x direction. The inner and outer heights of hollow SiO_2 are $h_2 = 2.6$ μm and $h_1 = 3$ μm. The inner and outer widths of the patterned SiO_2 are $w_2 = 3.5$ μm and $w_1 = 7$ μm. The tilted angle off the x axis is taken as θ. Here it is set as 63°. The thicknesses of the Si_3N_4 and Ag films are $h_3 = 0.8$ μm and $h_4 = 0.2$ μm, respectively. The absorption spectra and field distribution are numerically investigated with the finite difference time domain method. The incident plane electromagnetic wave is in the z direction and the electric field polarization is along x direction. A perfectly matched layer (PML) is set surrounding the unit cell in the z direction. The periodic boundary condition is applied along the x and y directions. The mesh size of each layer is 20 nm in the z direction and 50 nm in the x and y directions. The refractive index of Si_3N_4 and SiO_2 are obtained from the reference data.[37,38] The dielectric properties of the silver film are taken from Ref. [38]. With the solutions of Maxwell's equations on electromagnetic waves, we can finally obtain the optical spectrum. To obtain our designed metamaterials in the lab, silicon can be employed as the substrate of the radiative cooler and it does not influence the optical properties of the upper structure. The silver layer was firstly deposited on the silicon wafer by using dc magnetron sputtering, and then layers of Si_3N_4 and SiO_2 were deposited.[39] After that, an array of grooves on the top of the SiO_2 layer could be fabricated with lithography and the inductively coupled plasma reactive ion etching method.[40] A sacrificial layer was deposited on the silica layer to obtain the triangular prism patterns through the lithography and wet-etching process.[41] Then, a SiO_2 layer was deposited on the triangular prism patterns and the sacrificial layer etched away with a specific solution to get the hollow zigzag SiO_2 metamaterials.

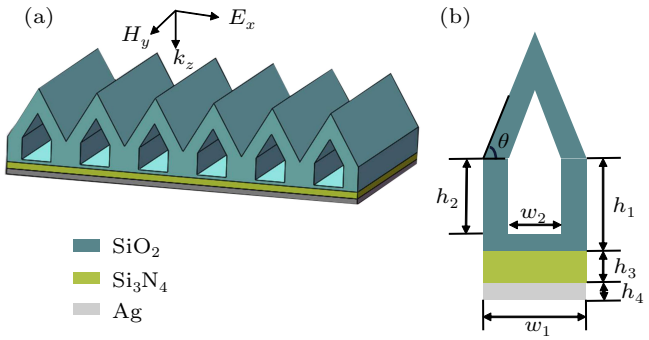


Fig. 1. Schematic diagram of thermal metamaterials. (a) 3D illustration. (b) Crosssection view. Parameters: h_1 =3 μm, $h_2 = 2.6$ μm, $h_3 = 0.8$ μm, $h_4 = 0.2$ μm, $w_1 = 7$ μm, $w_2 = 3.5$ μm, $\theta = 63°$.

2.2. Radiative cooling power

In order to evaluate the cooling performance of the thermal emitter, it is necessary to obtain its net cooling power (P_{net}). Usually, it is determined by four factors in the daytime environment. Namely, the infrared radiation of radiative cooler, solar irradiance, atmospheric thermal radiation and non-radiative radiation. The net radiative cooling power P_{net} is defined as[42]

$$P_{\text{net}} = P_{\text{rad}} - P_{\text{atm}} - P_{\text{sun}} - P_{\text{cond+conv}}, \tag{1}$$

where P_{rad} is the radiation power of the radiative cooler surface

$$P_{\text{rad}}(T) = A\int_0^{2\pi} \mathrm{d}\Omega \cos\theta \int_0^{\infty} \mathrm{d}\lambda I_{\text{B}}(T,\lambda)\varepsilon(\lambda,\theta), \tag{2}$$

P_{atm} is the absorbed power from the atmospheric thermal radiation

$$P_{\text{atm}}(T_{\text{amb}}) = A\int_0^{2\pi} \mathrm{d}\Omega \cos\theta \int_0^{\infty} \mathrm{d}\lambda I_{\text{B}}(T_{\text{amb}},\lambda)\varepsilon(\lambda,\theta)\varepsilon_{\text{atm}}(\lambda,\theta), \tag{3}$$

P_{sun} is the absorbed sun power

$$P_{\text{sun}} = A\int_0^{\infty} \varepsilon(\lambda,\theta) I_{\text{AM1.5}} \mathrm{d}\lambda, \tag{4}$$

$P_{\text{cond+conv}}$ is the power absorbed by conduction and convection

$$P_{\text{cond+conv}}(T, T_{\text{amb}}) = Ah_{\text{c}}(T_{\text{amb}} - T). \quad (5)$$

Here T_{amb} is the ambient temperature, T is the radiator surface temperature. $I_{\text{B}} = (2hc^2/\lambda^5)/[e^{hc/k_{\text{B}}T} - 1]$ stands for the blackbody radiation and $\varepsilon_{\text{atm}}(\lambda, \theta) = 1 - t(\lambda)^{1/\cos(\theta)}$ is the angular atmospheric emissivity. h, c, k_{B}, and h_{c} indicate the Planck constant, the speed of light, Boltzmann's constant, and the heat transfer coefficient, respectively. $\varepsilon(\lambda, \theta)$ is the emissivity of the film and A is the surface area of the radiative cooler. According to Kirchhoff's law, the absorptivity of an object is equivalent to emissivity in a thermodynamic equilibrium state. The mean solar reflectivity and emissivity can be obtained with the integral formula.[43] The column water vapor is assumed to be 1.0 mm and the air mass is 1.0 in this calculation. The global AM1.5 solar spectrum in Eq. (4) is 987 W·m^{-2} of direct normal irradiance.[44] The ambient temperature is taken as 300 K in our analysis.

3. Results and discussion

The absorption spectra of our designed radiative cooler as a function of the incident wavelength from 0.3 μm to 15 μm is shown in Fig. 2. It can be clearly observed that the proposed structure can simultaneously achieve high reflection in the solar band and high emission in the atmospheric window. In addition, the average emissivity is as high as 98.7% near the atmospheric window, which enables the structure to radiative cool maximally. Yellow and cyan colored spectra indicate AM1.5 solar power density and atmospheric transmittance in the atmospheric transparency window for reference. It illustrates that the radiative cooler has a broad near-unit absorptivity region in the atmospheric window embodying high performance for daytime radiative cooling.

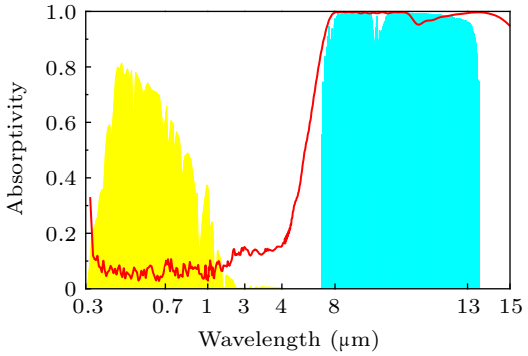


Fig. 2. Absorptivity of the hollow zigzag SiO_2 thermal metamaterials in the wavelength from 0.3 μm to 15 μm. Parameters: $w_1 = 7$ μm, $h_2 = 2.6$ μm, $\theta = 63°$. Emissivity curve of the radiative cooler (red), the scaled AM1.5 solar spectrum (yellow) and the atmospheric absorption spectrum (cyan) are plotted for reference.

To fully explore the physical origin of the high absorption in the atmospheric window, the resonant positions are marked in the absorptivity spectrum in Fig. 3(a). It is clearly found the minimum absorptivity is still around 0.95 in the atmospheric window. The electric field distribution at resonant positions of 8.1 μm, 8.7 μm, 9.3 μm, 10.0 μm and 11.1 μm are illustrated in Fig. 3(b) (*I*–*V*). The electric field mainly focuses on the top of the hollow zigzag structure at 8.1 μm in Fig. 3(I). It moves to the lateral sides of the hollow zigzag structure in the lower position as shown in Fig. 3(II). The electric field is confined around the two lateral regions in Fig. 3(III) at the resonant peak 10.0 μm. However, it penetrates the cavity in Fig. 3(IV).

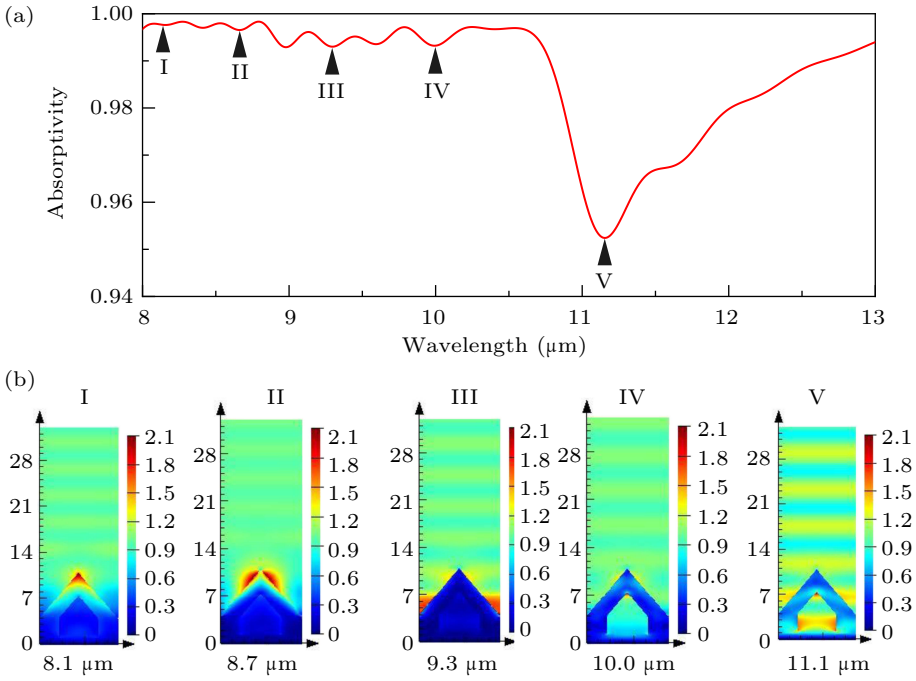


Fig. 3. (a) The absorption spectra of the thermal metamaterial with the resonant positions are marked with I, II, III, IV, and V. (b) The electric field distributions at (I) 8.1 μm, (II) 8.7 μm, (III) 9.3 μm, (IV) 10.0 μm, (V) 11.1 μm. Parameters: $w_1 = 7$ μm, $\theta = 63°$, $h_2 = 2.6$ μm.

At a larger resonant wavelength of 11.1 μm, the electric field intensity in the cavity gradually decreases. The intensity at resonant peak position V is less than that of (I, II, III and IV), indicating that the hollow zigzag structure plays a major role in the overall enhanced absorption. The graded refractive index (moth eye effects) can be employed to explain the high absorptivity in the atmospheric window.[29] The hollow zigzag structure can be viewed as an infinite number of thin layers. The index of each thin layer is lower than the lower adjacent layer when the groove width of the air decreases. Thus, the effective refractive index of the material changes continuously along the depth direction and a multilayer antireflective constitution occurs.[45–48] The imaginary part of the dielectric constant in Si_3N_4 and SiO_2 is extremely low in the solar region. Therefore, the reflectivity is not affected by the thickness of SiO_2.

Figure 4 presents the absorptivity in our designed metamaterials with different geometric parameters. Here the structure width is taken as 7 μm and $\theta = 63°$. With the increase of h_2 from 2.0 μm to 2.4 μm, the absorption spectrums shift to the high frequency region. To better reflect the tendency of the absorptivity, the average emissivity with different depths is shown in Fig. 4(b). With a larger h_2, the average emissivity first increases and then decreases. It reaches a maximum value at 2.6 μm. The relevant net cooling power at different depths is shown in Fig. 4(c). The trend of cooling power is consistent with the average emissivity and reaches the highest value of 100.6 $W{\cdot}m^{-2}$ at 2.6 μm. The dependence of the absorption spectrum with different θ is shown in Fig. 4(d). The absorptivity is above 92% in the atmospheric window. With a larger angle, the enhanced electric field around the edges is no longer the same. The electric field inside the cavity varies as well. Therefore, the absorptivity no longer overlaps in the wavelength ranging from 8 μm to 13 μm. To clearly reveal the influence of the angle θ, the average emissivity with different θ is illustrated in Fig. 4(e). The average emissivity increases from 50° to 63° and then decreases from 63° to 70° with an angle interval of 2°. The average emissivity and cooling power of the absorber are closely related to the width w_1 in Fig. 4(g). When $w_1$is taken from 3 μm to 7 μm, the emissivity is getting larger in Fig. 4(h). The net cooling power with different w_1 follows the same trend in Fig. 4(i). When w_1 is getting larger, the emissivity increases as well. Therefore, the optical geometry parameters can be obtained to get the desired emissivity in the atmospheric transparency window.

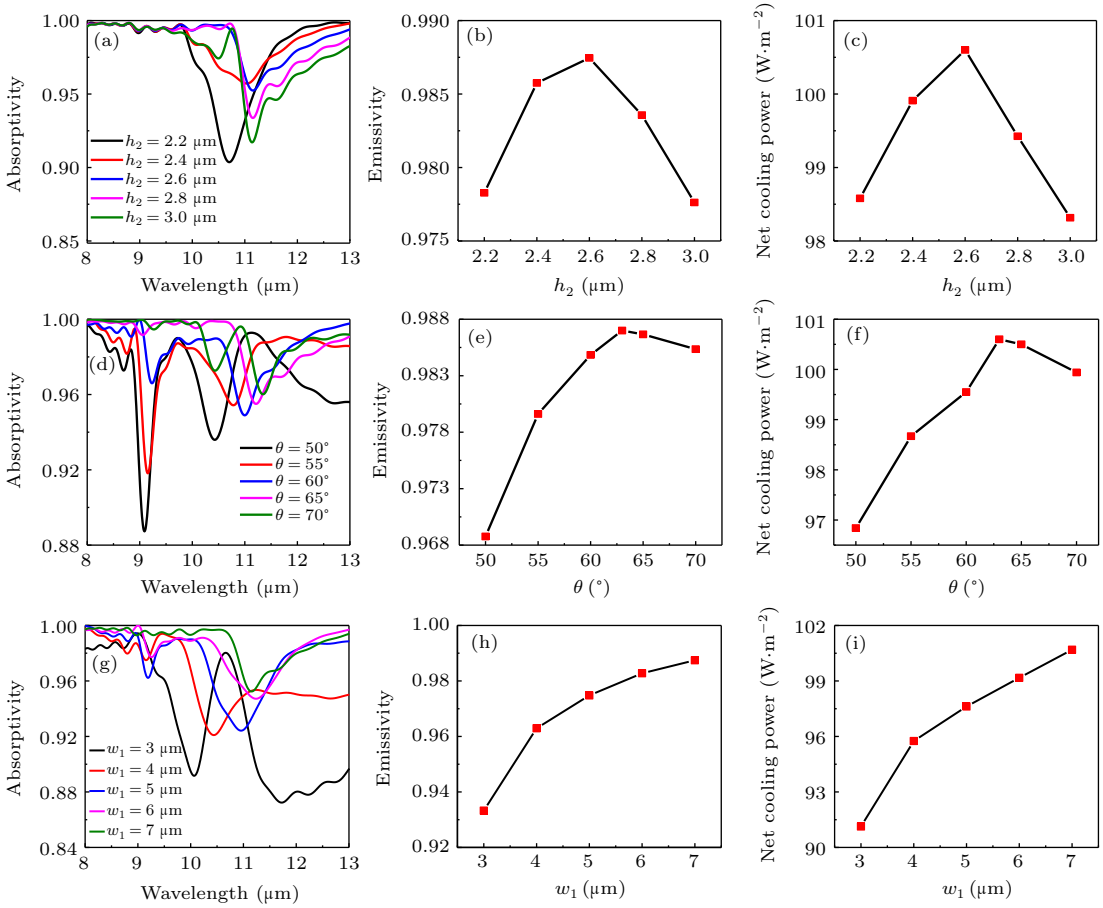


Fig. 4. (a) Absorptivity with different depths h_2. (b) The emissivity in relation with different depths. (c) Net cooling power with different depths. Parameters: $w_1 = 7$ μm, $\theta = 63°$. (d) Absorptivity with different angles θ. (e) The emissivity with different angle θ. (f) Net cooling power in relation with different angles θ. Parameters: $w_1 = 7$ μm, $h_2 = 2.6$ μm. (g) Absorptivity with different widths w_1. (h) The emissivity with different widths w_1. (i) Net cooling power with different widths w_1. Parameters: $h_2 = 2.6$ μm, $\theta = 63°$. The ambient temperature is 300 K.

It should be pointed out that the tunable emissivity can be achieved with different incident angle. Thus, the effect of incident angle on emissivity is taken into consideration in Fig. 5. This is more in line with the fact that the position of the sun changes every day. The high average emissivity is approaching 1.0 and it keeps as a constant between 0° and 30°. When the incident angle exceeds 60°, the average emissivity drops gradually. However, the average emissivity remains above 0.83. Namely, the emissivity can persist above 0.83 for angles of incidence less than 80°. Our results demonstrate that the proposed emitter can absorb the energy of incident wave almost perfectly with incident angle smaller than 80°, embodying excellent radiation performance in the atmospheric transparency window.

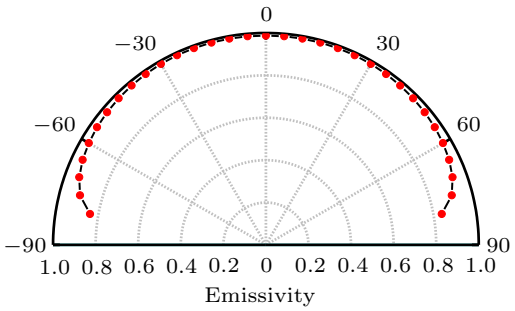


Fig. 5. Emissivity as a function of various incident angles in the atmospheric transparency window.

The net cooling power of our proposed structure as a function of emitter surface temperature T is demonstrated in Fig. 6. The influence of parasitic convection and conduction are in the absence (red curve). The net cooling power of the radiative cooler is 100.6 W·m^{-2} at the ambient temperature 300 K, which is due to its near-ideal emissivity and excellent heat dissipation performance in the atmospheric window. Moreover, the radiative cooler can reach an extremely low equilibrium temperature at 257 K. The influence of the non-radiative heat exchange coefficients is also taken into consideration. Here the coefficient is taken as h_c = 3, 6, 9 (W·m^{-2}·K^{-1}). With the increased h_c, the cooling power decreases rapidly when it is lower than the ambient temperature. Especially, the cooling effect persists even with a larger h_c.

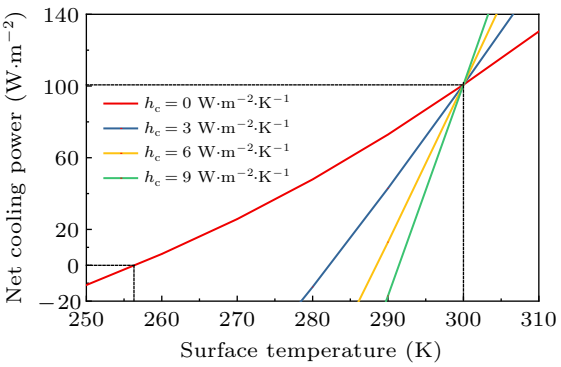


Fig. 6. The net cooling power of the proposed cooler with different h_c.

The net cooling power of the proposed cooler with different non-radiative heat exchange coefficients in Fig. 6 represents a steady-state process. However, the transient process of the radiative cooler under ambient temperature conditions is demonstrated in Fig. 7, which can be obtained by solving the differential equation[49]

$$C_{\text{cooler}}\frac{\mathrm{d}T}{\mathrm{d}t} = P_{\text{rad}} - P_{\text{atm}} - P_{\text{sun}} - P_{\text{cond+conv}}, \tag{6}$$

where C_{cooler} represents the heat capacitance and determined from the sum rule of multilayer design. The initial temperatures of the radiative cooler and ambient temperature are taken as the same. Here h_c is set as 6 W·m^{-2}·K^{-1}. The temperature variation of the radiative cooler as a function of time at different ambient temperatures is shown in Fig. 7(a). When the ambient temperature is 280 K, the cooling capacity of the radiative cooler is very limited. With the increase of the ambient temperature to 300 K, the cooling capacity of the radiative cooler increases to a value of 13 °C. An obvious drop of the temperature is found when the ambient temperature is 320 K. It indicates that the surface temperature of the radiant cooler finally decreases to 287 K, verifying the cooling ability of our designed cooler. Considering the transient process, the radiative cooling power versus time is considered in Fig. 7(b). It verifies that our designed emitter has excellent cooling performance. Meanwhile, the net radiative cooling power (P_{net}) shown with the blue line and radiative power (P_{rad}) in red gradually decrease with time. When the equilibrium process is approached, the net radiative cooling power becomes 0 and the radiative power is 165 W·m^{-2}, which is employed to eliminate the non-radiative radiation and the absorbed sun power.

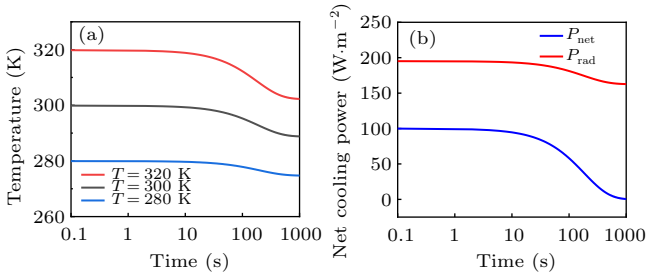


Fig. 7. Temperature evolution of the radiative cooler versus time at 280 K, 300 K and 320 K ambient temperature. (b) P_{rad} and P_{net} of the radiative cooler versus time under 300 K ambient temperature.

4. Conclusions

In summary, we have numerically described and investigated the emission properties of hollow zigzag SiO_2 metamaterials to achieve efficient daytime radiative cooling. A broadband absorption in the atmospheric window and a high reflectivity in the solar spectral can be simultaneously achieved. It can be analyzed with electric distribution and it originates from the graded refractive index of the hollow zigzag structure. The effects of the structure width w_1, the depth of the

groove h_2, the degree of zigzag θ and incident angle on the absorptivity are fully analyzed. Moreover, tunable ideal emissivity can be maintained at large angles, which is a desirable feature in maximizing the cooling power. The hollow zigzag SiO_2 metamaterial structure can achieve 100.6 $W{\cdot}m^{-2}$ and a drop of 13 °C for daytime cooling. When non-radiative exchange is considered, the proposed radiative cooler can still achieve effective cooling. Therefore, the designed structure not only provides potential applications in the radiative cooling system of buildings, solar cells and sensors, but also provides an insight into designing radiative coolers and related photonic structures.

References

[1] Hossain M M and Gu M 2016 *Adv. Sci.* **3** 1500360
[2] Zhao B, Hu M, Ao X, Chen N and Pei G 2019 *Appl. Energ.* **236** 489
[3] Chen S H, Wang X X, Nie G D, Liu Q, Sui j X, Song C, Zhu J W, Fu j, Zhang j C, Yan X and Long Y Z 2019 *Chin. Phys. B* **28** 064401
[4] Catalanotti S, Cuomo V, Piro G, Ruggi D, Silvestrini V and Troise G 1975 *Sol. Energy* **17** 83
[5] Granqvist C G and Hjortsberg A 1980 *Appl. Phys. Lett.* **36** 139
[6] Granqvist C G 1981 *Appl. Opt.* **20** 2606
[7] Granqvist C G and Hjortsberg A 1981 *J. Appl. Phys.* **52** 4205
[8] Suryawanshi C N and Lin C T 2009 *ACS. Appl. Mater. Inter.* **1** 1334
[9] Hossain M M, Jia B and Gu M 2015 *Adv. Opt. Mater.* **3** 1047
[10] Hannah K and Andrej L 2018 *J. Opt.* **20** 084002
[11] Ko B, Lee D, Badloe T and Rho J 2018 *Energies* **12** 89
[12] Bao H, Yan C, Wang B, Fang X, Zhao C Y and Ruan X 2017 *Sol. Energy. Mater. Sol. Cells* **168** 78
[13] Suichi T, Ishikawa A, Hayashi Y and Tsuruta K 2018 *AIP. Advances* **8** 055124
[14] Wu J Y, Gong Y Z, Huang P R, Ma G J and Dai Q F 2017 *Chin. Phys. B* **26** 104201
[15] Fan C Z, Gao Y and Huang J P 2008 *Appl. Phys. Lett.* **92** 251907
[16] Wang J Q, Fan C Z, He J N, Ding P, Liang E J and Xue Q Z 2013 *Opt. Express* **21** 2236
[17] Fan C Z, Ren P W, Jia W, Jia Y L and Wang J Q 2019 *Superlattice. Microst.* **136** 106295
[18] Ren P W, Jia Y L, Jia W and Fan C Z 2019 *J. Opt.* **21** 105101
[19] Zhao D, Aili A, Zhai Y, Lu J, Kidd D, Tan G, Yin X and Yang R 2019 *Joule.* **3** 111
[20] Cheng Z M, Wang F Q, Gony D Y, Liang H X and Shuai Y 2020 *Sol. Energy. Mater. Sol. Cells* **213** 110563
[21] Rephaeli E, Raman A and Fan S 2013 *Nano Lett.* **13** 1457
[22] Raman A P, Anoma M A, Zhu L, Rephaeli E and Fan S 2014 *Nature* **515** 540
[23] Chen Z, Zhu L X, Raman A and Fan S H 2016 *Nat. Commun.* **7** 13729
[24] Kecebas M A, Menguc M P, Kosar A and Sendur K 2017 *J. Quant. Spectrosc. Radiat. Transf.* **198** 179
[25] Jeong S Y, Tso C Y, Ha J, Wong Y M, Chao C Y H, Huang B and Qiu H 2020 *Renew. Energ.* **146** 44
[26] Kou J, Jurado Z, Chen Z, Fan S and Minnich A J 2017 *ACS. Photonics.* **4** 626
[27] Suichi T, Ishikawa A, Hayashi Y and Tsuruta K 2018 *AIP. Advances* **8** 055124
[28] Yang P, Chen C and Zhang Z M 2018 *Sol. Energy* **169** 316
[29] Wu D, Liu C, Xu Z, Liu Y, Yu Z, Yu L, Chen L, Li R, Ma R and Ye H 2018 *Mater. Design* **139** 104
[30] Zhu L, Raman A. Wang K X, Anoma M A and Fan S 2014 *Optica* **1** 32
[31] Jeong S Y, Tso C Y, Wong Y M, Chao C Y H and Huang B 2020 *Sol. Energy. Mater. Sol. Cells* **206** 110296
[32] Gentle A R and Smith G B 2010 *Nano. Lett.* **10** 373
[33] Huang Z and Ruan X 2017 *Int. J. Heat. Mass. Tran.* **104** 890
[34] Zhai Y, Ma Y G, David S N, Zhao D L, Lou R N, Tan G, Yang R G and Yin X B 2017 *Science* **355** 1062
[35] Fu Y, Yang J, Su Y S, Du W and Ma Y G 2019 *Sol. Energy. Mater. Sol. Cells* **191** 50
[36] Chae D, Kim M, Jung P H, Son S, Seo J, Liu Y, Lee B J and Lee H 2020 *ACS. Appl. Mater. Inter.* **12** 8073
[37] Kischkat J, Peters S, Gruska B, Semtsiv M, Chashnikova M, Klinkmüller M, Fedosenko M, Machulik S, Aleksandrova A, Monastyrskyi G, Flores Y and Masselink T 2012 *Appl. Optics* **51** 6789
[38] Palik E 1998 *Handbook of Optical Constants of Solids* (Vol.1) (New York: Harcourt Brace Jovanovich) pp.749–763
[39] Cunha N F, AL-Rjoub A, Rebouta L, Vieira L G and Lanceros-Mendez 2020 *Thin Solid Films* **694** 137736
[40] Fukasawa T, Kubota K, Shindo H and Horiike Y 1994 *Jpn. J. Appl. Phys.* **33** 7042
[41] Kumar M D, Kim H and Kim J 2015 *Sol. Energy* **117** 180
[42] Wu J Y, Gong Y Z, Huang P R, Ma G J and Dai Q F 2017 *Chin. Phys. B* **26** 213
[43] Li N, Wang J, Liu D, Huang X, Xu Z, Zhang C, Zhang Z and Zhong M 2019 *Sol. Energy. Mater. Sol. Cells* **194** 103
[44] Air mass 1.0 spectra, American Society for Testing and Materials (ASTM) http://rredc.nrel.gov/solar/spectra/am1.5/ (Available from)
[45] Lou S, Guo X, Fan T and Zhang D 2012 *Energ. Environ. Sci.* **5** 9195
[46] Kong A, Cai B, Shi P and Yuan X C 2019 *Opt. Express* **27** 30102
[47] Fan C Z, Wang J Q, Zhu S M, He J N, Ding P and Liang E J 2013 *J. Opt.* **15** 055103
[48] Fan C Z, Wang J Q, Cheng Y G, Ding P, Liang E J and Huang J P 2013 *Chin. Phys. B* **22** 084703
[49] Ono M, Chen K, Li W and Fan S H 2018 *Opt. Express* **26** A777